Reprinted from JOURNAL OF APPLIED PHYSICS, Vol. 33, No. 7, 2275–2282, July, 1962

Printed in U. S. A.

Determination of Plasma Properties by Free-Space Microwave Techniques

R. BUSER AND W. BUSER
U. S. Army Signal Research and Development Laboratory, Fort Monmouth, New Jersey
(Received October 25, 1961)

Time-resolved free-space microwave measurements are used to study the loss mechanisms in the afterglow of an intense He discharge between 100 and 1000 μ. The method of evaluation is developed in detail and the results of the measurements and their accuracy are given. Some of the problems and limitations of the microwave method are discussed; in particular, plots of the field pattern between the horns are presented indicating that a reasonable interpretation in terms of an integrated path length is possible.

INTRODUCTION

THE free transmission of a microwave signal through a gas discharge provides a very useful tool for the study of electron loss processes. Many applications have been reported in connection with plasma research mainly used to calculate the electron density.[1–5] Because of the complexity of the possible processes involved in a time-varying plasma, however, one commonly resorts to approximations and simplifications, which are not easy to justify. Since, in addition, the plasma is in many cases located in the near-field zone of the transmitting and receiving horns (an area where the field pattern is complex) it is not immediately apparent that a reasonable interpretation of the measurements is possible.

This paper reports an attempt to improve the interpretation of free-space microwave measurements. We first explored how the electron decay mechanisms (ambipolar diffusion, volume recombination, and attachment) are connected with the quantity measured, namely, the integral index of refraction (optical path) and its change with time. We then applied the theory to measurements made on a pulsed high current He discharge. We found that either ambipolar diffusion or attachment, or both, provide a good explanation for the measured electron decay. Additional experiments with a magnetic field may allow the separation of ambipolar diffusion from attachment. We finally discuss the validity of an important assumption, namely, the plane wave condition, which is necessary for a detailed interpretation of the measurement.

EXPERIMENTAL PROCEDURE

The Discharge System

The discharge circuit is composed of a plasma container 90 cm high and 7.1 cm in inner radius (consisting of a Pyrex glass tube with stainless steel electrodes), a coaxial airgap switch with a trigger electrode, a 15 000-J condenser bank, a power supply, and the necessary timing circuits (Fig. 1). Triggering of the airgap switch discharges the condensers, and a high current[6] (of the order of 10^5 A) is conducted through the discharge tube and creates a plasma, the properties of which depend on voltage, pressure, and gas used. After $\approx$100 μsec the discharge current ceases, after $\approx$1000 μsec the plasma becomes transmitting, and after several milliseconds,[7] the original state is reached again (Fig. 2).

Prior to the discharge the vessel was pumped out (oil diffusion pump with liquid nitrogen cold trap) and moderately baked for several hundred hours. "High" purity He[8] was then filled into the discharge tube. During the measurements, the relative intensity of certain impurity lines was monitored by a monochromator-photomultiplier system, showing weak lines (which we identified as nitrogen, oxygen, and iron) in a strong background continuum. Since the sensitivity of this system is limited, there may have been other impurities that we could not identify. The pressure range of all experiments was between 100 and 1000 μ, the lower limit given by the maximum permissible voltage on the condensers (20 kV), and the upper limit given by the "noisiness" of the records, indicating turbulent motion at the time of measurement. The pressure itself was measured by a thermocouple gauge,

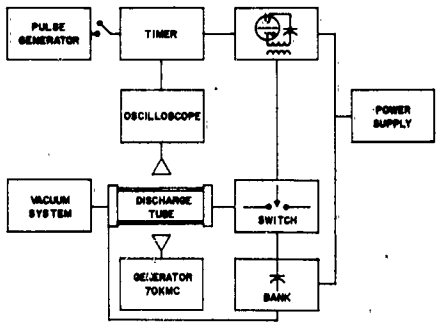

FIG. 1. Discharge system.

[1] R. F. Whitmer, Phys. Rev. **104**, 572 (1956).
[2] C. B. Wharton, *IV International Conference on Ionisation Phenomena in Gases* (North-Holland Publishing Company, Amsterdam, 1960), III C737.
[3] C. B. Wharton and D. M. Slager, J. Appl. Phys. **31**, 428 (1960).
[4] C. B. Wharton, Riso Report No. 18.
[5] V. E. Golant, J. Tech. Phys. (U.S.S.R.) **30**, 1265 (1960) [translation: Soviet Phys.—Tech. Phys. **5**, 1197 (1961)].

[6] Peak current $J_p \approx U_0 2\pi\nu C$, ν=33 kc, C=72 μF, U_0=voltage on the condensers.
[7] The measurement of pressure transients is explained in a note submitted to *The Review of Scientific Instruments*.
[8] Impurity content according to the manufacturer (Linde Company): <5 ppm O_2, <5 ppm H_2, <3 ppm H_2O, <50 ppm N_2.

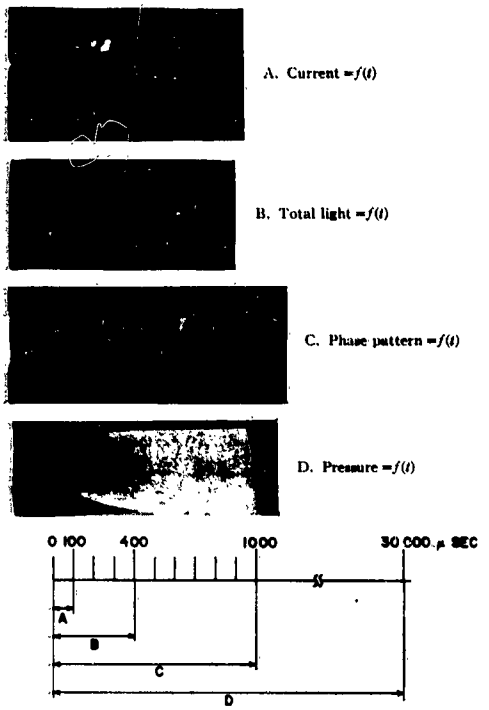

FIG. 2. Representative time sequence.

which had been calibrated for He by means of a McLeod gauge.

The Microwave Interferometer

The general setup of the microwave interferometer is well known (see Fig. 3 for the arrangement used in our experiment). The source energy (reflex klystron, 70 kMc, 50 mW) was divided into two paths: a measuring path, where a microwave beam interacts with the plasma, and a reference path. The relative change of phase produced by introduction of a time-varying plasma was then detected by a phase bridge, amplified, and recorded on two oscilloscopes with cameras attached, one giving an over-all pattern of the full phase cycle (heating and decay), and the other extracting by proper scope adjustment an enlarged "detail pattern" from the over-all pattern that permits a higher accuracy in the evaluation process. In addition to the phase measurement, we recorded the transmitted energy (intensity pattern), and checked periodically the reflected energy, the latter being generally very small.

The klystron was modulated with 4.5 Mc, and the amplifiers were resonance amplifiers tuned to 4.5 Mc with a bandwidth of approximately 400 kc. Use of a modulated interferometer circuit has some advantages: Even at a very low power output of the klystron, which is preferable in order to avoid any influence of the microwaves on the plasma, the signal can be sufficiently amplified without distortion by thermal noise. The adjustment of a particular zero phase was essentially very simple, and any changes of the zero phase in the course of a long series of measurements could easily be corrected. The change of phase due to the plasma appeared in this way as a modulation of the 4.5-Mc signal, and since the oscilloscope sweep was not synchronized with this latter frequency but chosen appropriate to the discharge mechanism, the phase change (and similarly the change of intensity of the transmitted wave) was given by the envelope of the record. An analysis of the errors introduced by use of a modulated phase bridge showed that these were negligible compared to those encountered in reading the records and to others that are discussed later.

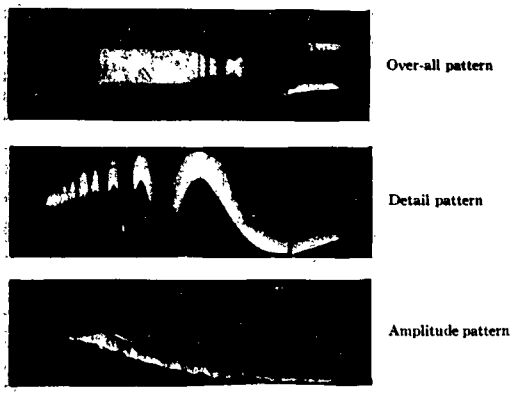

FIG. 4. Measurement of the propagation characteristics of a He plasma (voltage 5.3 kV, pressure 225 μ).

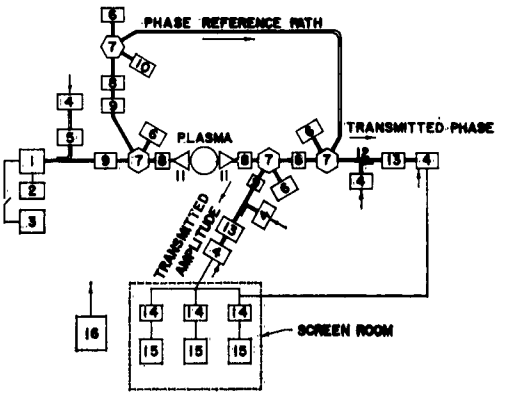

FIG. 3. Microwave setup for simultaneous measurement of transmitted phase and amplitude. 1. Klystron λ = 4 mm, 2. power supply, 3. modulator 1 kc or 4.5 Mc, 4. crystal detector, 5. wave meter, 6. termination, 7. hybrid, 8. isolator, 9. attenuator, 10. tuning stub, 11. horn, 12. directional coupler, 13. *E/H* tuner, 14. preamplifier, 15. oscilloscope, 16. VSWR receiver.

INTERPRETATION OF THE INTERFERENCE PHASE PATTERN

Proceeding in the manner described, we obtained three simultaneous measurements on the propagation characteristics of the plasma. Figure 4 shows an over-all pattern (actual interference pattern), a detail pattern of the interference measurement, and an intensity pattern of the transmitted wave, all as a function of time and representing a typical gas-discharge cycle. Each record also has time scales, and on some records, superimposed identification pips that give a fix-point in time on all three records. Since each record has its own time scale, we were able to correct for distortions caused by nonlinearities of the oscilloscopes.

Determination of the Integral Index of Refraction

We start with four assumptions. The plasma is a lossless medium, the wave transmitted and received by the horns is a plane wave, the diameter of the microwave beam is small in comparison to the plasma diameter and the index of refraction n changes slowly compared with the wavelength and reflection is therefore negligible. Our measurement then leads to an integral index of refraction as described below.

In Fig. 5 we show a schematic representation of the over-all pattern and the intensity pattern. Let t_l be the time of the lth extremum and (it is irrelevant which extremum is chosen to be the first one; l is only a running index) let t_k be the time of the last recorded extremum. Only at $t=\infty$ is n strictly 1 throughout the discharge tube. As can be seen from Fig. 4, however, phase and intensity of the measuring wave reach their final values soon after the last extremum. We have then the following set of equations expressing the phase angles in terms of the microwave vacuum wavelength λ_0:

$$\begin{aligned}
&\int_{-R}^{+R} n(t_\infty,r)dr-\int_{-R}^{+R} n(t_k,r)dr=\frac{\lambda_0}{2}\frac{\varphi_\infty}{2\pi}\\
&\int_{-R}^{+R} n(t_k,r)dr-\int_{-R}^{+R} n(t_{k-1},r)dr=\frac{\lambda_0}{2}\\
&\int_{-R}^{+R} n(t_{l+1},r)dr-\int_{-R}^{+R} n(t_l,r)dr=\frac{\lambda_0}{2},
\end{aligned} \tag{1}$$

where R=radius of the discharge tube, r=radial coordinate, t=time, and φ_∞=zero-density phase angle between reference and measuring wave at $t=\infty$.

Since

$$\int_{-R}^{+R} n(t_\infty,r)dr=2R, \tag{2}$$

$$\int_{-R}^{+R} n(t_l,r)dr=2R-\frac{\lambda_0}{2}\left[\frac{\varphi_\infty}{\pi}+(k-l)\right]. \tag{3}$$

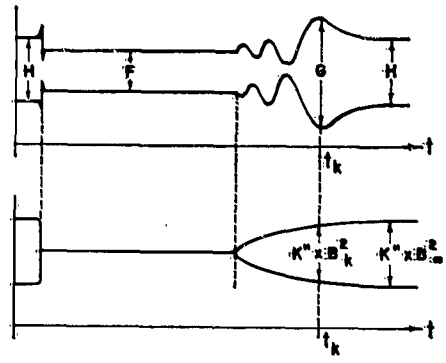

FIG. 5. Schematic representation of the phase and amplitude pattern.

Thus, Eq. (3) gives the integral refractive index as a function of time.

We derive the zero phase angle as follows (see Fig. 6). Let A=amplitude of reference wave, B=amplitude of measuring wave, and K'=constant of proportionality. Then these relations hold, if the detector follows a square-law relation[9]:

$$\begin{aligned}
&F=K'A^2\\
&G=K'(A+B)^2\\
&H=K'(A^2+B^2+2AB\cos\varphi_\infty),
\end{aligned} \tag{4}$$

(see Fig. 5), and

$$\cos\varphi_\infty=1-\frac{G/F-H/F}{2[(G/F)^{\frac{1}{2}}-1]}. \tag{5}$$

For high accuracy of the measurement of the zero-density phase angle, we see that it should be $\approx 90°$; this is approximately true if we choose $H\approx F$ and the latter can be adjusted very simply even without a calibrated phase shifter.

If we consider the plasma as a phase shifting and lossy medium (removing our first assumption), we

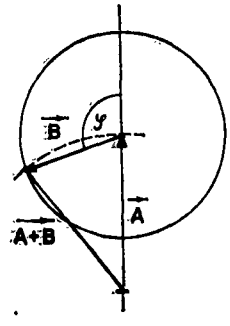

FIG. 6. Determination of the zero angle (lossless case).

[9] The detector used in these experiments very closely follows a square-law relation.

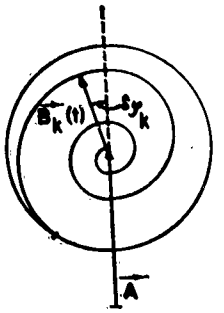

FIG. 7. Vector diagram for loss case.

replace Eq. (1) by:

$$\int_{-R}^{+R} n(l_\infty,r)dr-\int_{-R}^{+R} n(l_k,r)dr=\frac{\lambda_0}{2}\left(\frac{\varphi_\infty}{\pi}-\frac{\delta\varphi_k}{\pi}\right)$$

$$\int_{-R}^{+R} n(l_k,r)dr-\int_{-R}^{+R} n(l_{k-1},r)dr=\frac{\lambda_0}{2}\left(1+\frac{\delta\varphi_k}{\pi}-\frac{\delta\varphi_{k-1}}{\pi}\right)$$

$$\int_{-R}^{+R} n(l_{l+1},r)dr-\int_{-R}^{+R} n(l_l,r)dr=\frac{\lambda_0}{2}\left(1+\frac{\delta\varphi_{l+1}}{\pi}-\frac{\delta\varphi_l}{\pi}\right). \quad (6)$$

If we add and use Eq. (2), then

$$\int_{-R}^{+R} n(l_l,r)dr=2R-\frac{\lambda_0}{2}\left[\frac{\varphi_\infty}{\pi}+(k-l)-\frac{\delta\varphi_l}{\pi}\right], \quad (7)$$

where $\delta\varphi_l$ is the (generally small) angle caused by the increase of B with time (Fig. 7). Its magnitude depends on the rate of change of B and cannot be given without further analysis. If F, G, H, A, B_∞, B_k, and φ_∞ have the same meaning as explained before, we have

$$\begin{aligned} F&=K''A^2 \\ G&=K''(A^2+B_k^2+2AB_k\cos\delta\varphi_k) \\ H&=K''(A^2+B_\infty^2+2AB_\infty\cos\varphi_\infty). \end{aligned} \quad (8)$$

With $g=B_\infty/B_k$, there follows

$$\cos\varphi_\infty=\frac{H/F-1}{2g\{[G/F-(1-\cos^2\delta\varphi_k)]^{\frac{1}{2}}-\cos\delta\varphi_k\}} -g/2\{[G/F-(1-\cos^2\delta\varphi_k)]^{\frac{1}{2}}-\cos\delta\varphi_k\}. \quad (9)$$

As can be seen from Eq. (9), $\delta\varphi_k$ only appears as a second-order influence upon $\cos\varphi_\infty$ (provided that G is sufficiently greater than F) and moreover tends to cancel out. Since the rate of change of B in the neighborhood of t_k is small, $\delta\varphi_k$ will be quite small and we can substitute Eq. (10) for Eq. (9).

$$\cos\varphi_\infty=g\left\{\frac{G/F-\frac{1}{g^2}\cdot\frac{H}{F}+\frac{1}{g^2}-1}{1-\frac{1}{2[(G/F)^{\frac{1}{2}}-1]}}\right\} \quad (10)$$

which replaces Eq. (5).

Interpretation of the Phase Pattern Under the Assumption that Ambipolar Diffusion is the Dominant Loss Process

In the following analysis the simplified Eqs. (3) and (5) will be applied. The equation describing the electron density as a function of time and space is

$$\partial n_-/\partial t=D_A\nabla^2 n_-, \quad (11)$$

where n_- = number of electrons/cm^3 and D_A = ambipolar diffusion coefficient. If D_A is assumed to be constant with space and time, then the solution of Eq. (11) for cylindrical coordinates, considering only solutions symmetrical in θ is

$$n_-(l,r,z)=\sum_{\nu,\mu=1}^{\infty} C_{\nu\mu}'\exp\left(-\frac{l}{\tau_{\nu\mu}}\right)J_0\left(j_{0,\nu}\cdot\frac{r}{R}\right)\sin\left(\frac{\mu\pi z}{H}\right) \quad (12)$$

$$\frac{1}{\tau_{\nu\mu}}=D_A\left[\left(\frac{j_{0,\nu}}{R}\right)^2+\left(\frac{\mu\pi}{H}\right)^2\right]. \quad (13)$$

For the boundary condition

$$n_-(l,R,z)=n_-(l,r,0)=n_-(l,r,H)=0,$$

where H = height of discharge tube, z = axial coordinate, $C_{\nu\mu}'$ = constants given by the initial distribution, J_0 = Bessel function of order zero, and $j_{0,\nu}$ = its νth root. Since we always measure at $z=H/2$, that is, the middle of the discharge tube, and with the abbreviation of

$$J_0\left(j_{0,\nu}\frac{r}{R}\right) \quad \text{to} \quad J_0{}^\nu\left(\frac{r}{R}\right)$$

then Eq. (12) reduces to

$$n_-(l,r)=\sum_{\nu,\mu=1}^{\infty} C_{\nu\mu}'\exp\left(-\frac{l}{\tau_{\nu\mu}}\right)J_0{}^\nu\left(\frac{r}{R}\right)\sin\frac{\mu\pi}{2}. \quad (14)$$

For sufficiently large t, all the higher modes vanish, and the electron density is determined solely by the first mode. With $C_{11}'=C_1'$, $\tau_{11}=\tau_1$ we have

$$n_-(l,r)=C_1'\exp\left(-\frac{l}{\tau_1}\right)\cdot J_0'\left(\frac{r}{R}\right), \quad (15)$$

$$\frac{1}{\tau_1}=D_A\left[\left(\frac{j_{0,1}}{R}\right)+\left(\frac{\pi}{H}\right)^2\right]. \quad (16)$$

Let $C_1' \cdot K = C_1$, then with $n=[1-(\omega_0/\omega)^2]^{\frac{1}{2}}$, ω = angular frequency of the electromagnetic wave, and ω_0 = plasma frequency.[10]

$$n(t,r)=\left[1-\left(\frac{\omega_0}{\omega}\right)^2\right]^{\frac{1}{2}}=[1-n_-(t,r)\cdot K]^{\frac{1}{2}}$$

$$=\left[1-C_1\exp\left(-\frac{t}{\tau_1}\right)\cdot J_0'\left(\frac{r}{R}\right)\right]^{\frac{1}{2}}, \qquad (17)$$

and with $\alpha=C_1\exp(-t/\tau_1)$, $\alpha_l=C_1\exp(-t_l/\tau_1)$

$$\int_{-R}^{+R} n(t_l,r)dr=\int_{-R}^{+R}\left[1-\alpha_l\cdot J_0'\left(\frac{r}{R}\right)\right]^{\frac{1}{2}}dr. \qquad (18)$$

It is convenient to choose R as the unit of length, thereby simplifying Eq. (18) to

$$\int_{-1}^{+1} n(t_l,r)dr=\int_{-1}^{+1}[1-\alpha_l J_0'(r)]^{\frac{1}{2}}dr. \qquad (19)$$

The left side of Eq. (19) is known through Eqs. (3) and (5), each l and t_l, respectively, thereby determining one α_l. Because of $\alpha_l=C_1\exp(-t_l/\tau_1)$, we get

$$\ln\frac{0.6}{\alpha_l}=\frac{t_l}{\tau_1}+\ln\frac{0.6}{C_1}. \qquad (20)$$

(The constant 0.6 proves to be numerically convenient.) Plotting t_l vs $\ln 0.6/\alpha_l$, one should get a straight line whose slope yields τ_1 and D_A, and whose intercept yields $\ln 0.6/C_1$ and therefore C_1.

Interpretation of the Phase Pattern Under the Assumption that Ambipolar Diffusion and Electron Attachments are the Dominant Loss Processes

The equation which describes the time dependence of the electron density is as follows,

$$\partial n_-/\partial t=D_A\nabla^2 n_- -\beta n_- \qquad (21)$$

β = attachment frequency.

Again assuming that D_A and β are constant with space and time, the solution of Eq. (21) is the same as that of Eq. (11), except that

$$\frac{1}{\tau_{s\mu}}=\beta+D_A\left[\left(\frac{j_{0,s}}{R}\right)^2+\left(\frac{\mu\pi}{H}\right)^2\right]. \qquad (22)$$

All that has been said for Eqs. (12) and (13) applies here too. If it is possible to determine in an experiment a τ_1 and τ_2, D_A and β may be computed from Eq. (22). Another possibility is to measure $1/\tau$ as function of the magnetic field, which only influences the value of D_A but not β. It should be remembered, however, that strictly speaking, D_A has to be derived from a three-particle model, since attachement means that besides positive ions and electrons, negative ions are also present.[11] The above statement is true only if the concentration of negative ions is negligible.

Interpretation of the Phase Pattern Under the Assumption that Volume Recombination is the Dominant Loss Process

In this case it is

$$\partial n_-/\partial t=-\alpha_V n_-^2, \qquad (23)$$

where α_V is volume recombination coefficient.

If α_V is assumed to be constant, then the solution of Eq. (23) is

$$n_-=\rho(r)/[c+\alpha_V\rho(r)(t-t_0)], \qquad (24)$$

where c = constant and $\rho(r)/c$ = spatial distribution of the electrons at $t=t_0$. The spatial distribution of the electrons at some fixed time has to be known in order to evaluate Eq. (24). It could be known, for example, by some independent optical measurement. Since we do not know $\rho(r)$, however, we shall make two reasonable assumptions and check them against the experiment. While this method is not correct it should at least give an idea whether or not volume recombination is the dominant loss process. If we assume a homogenous distribution

$$\rho(r)=1 \quad 0\le r<R$$
$$=0 \quad r=R, \qquad (25)$$

and with Eq. (17)

$$\int_{-R}^{+R} n(t_l,r)dr=\int_{-R}^{+R}\left[1-\frac{K\cdot\rho}{c+\alpha_V\rho(t_l-t_0)}\right]^{\frac{1}{2}}dr=2RA_l, \qquad (26)$$

K = constant.

Again, the left side of Eq. (26) is known from Eqs. (3) and (7), each l and t_l determining uniquely one A_l. Furthermore, we have

$$1/(1-A_l^2)=\alpha_V t_l/K+[(c/\rho)-\alpha_V t_0]/K. \qquad (27)$$

Plotting t_l vs $(1-A_l^2)^{-1}$ one should get a straight line, whose slope yields K/α_V and therefore α_V.

If we assume a Bessel function for the spatial distribution

$$\rho(r)=J_0\left(j_{0,1}\cdot\frac{r}{R}\right)=J_0'(r), \qquad (28)$$

and

$$\int_{-R}^{+R} n(t_l,r)dr=\int_{-R}^{+R}\left[1-\frac{KJ_0'(r)}{c+\alpha_V J_0'(r)\cdot(t_l-t_0)}\right]^{\frac{1}{2}}dr. \qquad (29)$$

We choose $t_0=t_k$, thereby determining c since the left

[10] The use of this equation is consistent with the use of Eqs. (3) and (5), wherein the plasma is considered to be a lossless medium.

[11] H. J. Oskam, Phillips Research Repts. 13, 335 (1958).

side of Eq. (29) is known for every l. Let

$$(\alpha_V/c)(t_l-t_k)=B_l, \tag{30}$$

then

$$\int_{-R}^{+R} n(l,r)dr=\int_{-R}^{+R}\left[1-\frac{K/c}{1/J_0'(\tau)+B_l}\right]^{\frac{1}{2}}dr. \tag{31}$$

Each l and t_l corresponds uniquely to one B_l. Plotting t_l vs B_l one should get a straight line whose slope is c/α_V and therefore yields α_V.

If ambipolar diffusion and volume recombination are the dominating loss processes, the differential equation cannot generally be solved.

EVALUATION OF PHASE RECORDS, ESTIMATE OF ERRORS

The positions of the extrema on the phase pattern were measured with a thread mark moved by a micrometer. In the same way the time marks on each picture were measured whose distances were known to be exactly 100 μsec. Thus the relative positions of the extrema were obtained in μsec, and nonlinearities of the oscilloscope or distortions of the photograph were eliminated. The error in defining the position of an extremum generally did not exceed ±5 μsec, the last extremum being an exception. Because of its flattened shape, the reading error was about ±25 to 50 μsec. The next step was to compute the zero angle φ_∞ [Eq. (5) or (10)]. We found that g [Eq. (10)] was very close to 1 within the limited accuracy with which the intensity pattern could be read because of its ripples: Therefore Eq. (5) was used. The error in computing φ_∞ was $\leq\pm5°$. Next, α_l had to be determined from Eq. (19). Based on a computer calculation $\ln 0.6/\alpha_l$ was plotted against

$$\int_{-1}^{+1}[1-\alpha J_0'(\tau)]^{\frac{1}{2}}dr=\int_{-1}^{+1}n(l,r)dr,$$

and since

$$\int_{-1}^{+1}n(l,r)dr=2R-\frac{\lambda_0}{2}\left[\frac{\varphi_\infty}{\pi}+(k-l)\right],$$

$\ln 0.6/\alpha_l$ could be simply read off the plot for every l and t_k. Finally t_l was plotted against $\ln 0.6/\alpha_l$, the slope giving τ_1. The error in determining $\ln 0.6/\alpha_l$ arises from the inaccuracy of φ_∞ and is generally $<\pm0.05$ for $l=k$, ±0.02 for $l=\frac{1}{2}-1$ and successively smaller for decreasing l. Since the last point ($l=k$) is the most unreliable, the slope of t_l plotted against $\ln 0.6/\alpha_l$ was determined from the next-to-last points. Figure 8 is a representative example. It can be seen that there is a systematic error insofar as all maxima ($l=k, k-2, \cdots$) and all minima lie on a straight but slightly different line. The cause of this error in the electronic circuit and has not yet been remedied. Therefore the slope was determined from an interpolation between maxima and minima, as shown in Fig. 8. It can also be seen that the points deviate slightly from the straight line, and the possible causes of this will be discussed later. The error in computing τ_1 does not exceed ±2%.

RESULTS AND DISCUSSION

In Fig. 9, we give a typical representation of the records in terms of volume recombination, assuming a homogeneous or a Bessel function type distribution of the plasma across the discharge tube [Eqs. (26) and (31)]. In Fig. 8 we show the same record interpreted in terms of ambipolar diffusion and attachment [Eqs. (18) and (22)]. Many data of the type given in Fig. 8 have been evaluated. In Table I for example, we checked the question of reproducibility (maximum differences of $1/\tau_1$ are in the order of 3%). In Table II

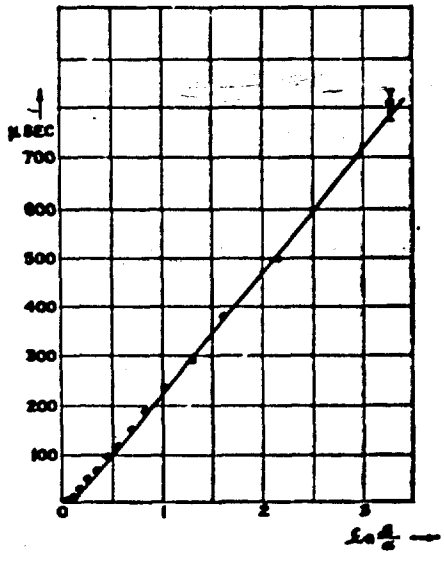

FIG. 8. Typical representation for plot of t vs $\ln 0.6/\alpha$; $\tau_1=2.49\cdot10^{-4}$ (Ambipolar diffusion and attachment).

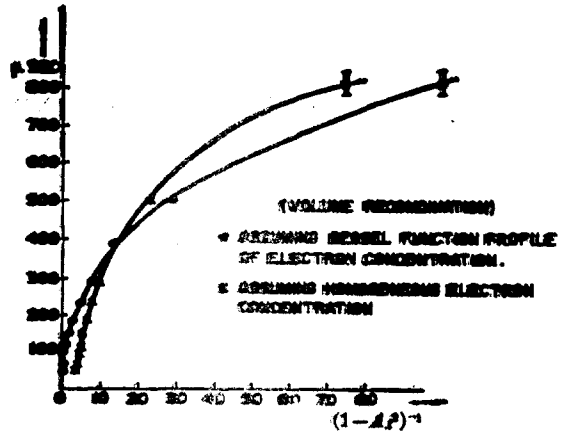

FIG. 9. Typical representation for plot of t vs $(1-A\beta^2)^{-1}$.

TABLE I. Reproducibility of measurements.

p(μ)	U(kV)	$1/\tau_1$
225	5.3	4.115×10³
225	5.3	4.086×10³
225	5.3	4.065×10³
225	5.3	4.000×10³
225	5.3	4.046×10³
225	5.3	4.082×10³
225	5.3	4.000×10³

TABLE II. Pressure dependence.

p(μ)	U(kV)	$1/\tau_1$
575	4.8	2.778×10³
465	4.8	2.551×10³
365	4.8	2.801×10³
230	4.8	3.425×10³

we show a few measurements in which we studied the pressure dependence.

The results of the measurements so far indicate the following:

(a) Volume recombination cannot be a major loss mechanism (Fig. 9, where we should find a straight line). This is in agreement with other measurements in He discharges in the late afterglow.[12]

(b) The measurements can be fairly well interpreted by either ambipolar diffusion or attachment, or both (Fig. 8), the latter being most probable.

One way to assess the importance of both effects is to study their dependence on a magnetic field. According to the classical theory[13]:

$$D_A = D_A(H^{-2}), \quad \beta \neq \beta(H). \tag{32}$$

H = magnetic field, and accordingly (in the presence of an axial field)

$$\frac{1}{\tau_1} = D_A^M\left(\left(\frac{j_{0,1}}{R}\right)^2 + D_A\left(\frac{\pi}{H}\right)^2 + \beta. \right. \tag{33}$$

(D_A^M = ambipolar diffusion with magnetic field.) Obviously, any dependence of $1/\tau_1$ on the magnetic field H will indicate ambipolar diffusion. Some preliminary measurements with axial magnetic fields show indeed a marked influence and lead to $D_A \approx 5000$ and $\beta \approx 1000$ (indicating a high degree of impurities). The assumption here is, that the initial conditions of the gas discharge are essentially unchanged.

If we then take for D_A a value of the order of 5000 cm²/sec we have, if electron temperature T_- and ion temperature T_+ are equal,[11]

$$D_A = D_+(T_+)\left(\left(1+\frac{T_-}{T_+}\right)\right) = 2D_+(T_+), \tag{34}$$

$$D_+ = (\mu_+ kT_+)/e \sim T_+ \approx T_{\text{gas}}, \tag{35}$$

(assuming the ion mobility μ_+ temperature independent) and therefore

$$D_A(T_1)/D_A(T_2) = T_1/T_2. \tag{36}$$

If we use $D_A p \approx 600$ (cm²/sec mm Hg) at 300°K from the literature, we obtain $T \approx 750$°K. Many more measurements are necessary to determine the accuracy of these calculations.

(c) According to Eq. (20) a plot of t_l vs $\ln 0.6/\alpha_l$ should be a straight line for late times. The results given in Fig. 8 show a slight curvature, however. In our interpretation [(b) above], this could be attributed to the change of D_A and β with temperature and therefore with time. Equation (21) should read

$$\partial n_-/\partial t = D_A(t)\nabla^2 n_- - \beta(t) n_-. \tag{37}$$

It is easy to show that the change of the slope in connection with this effect goes in the right direction. In this way, the changing slope could indicate the change of D_A and β with temperature. The same effect could also be due to higher diffusion modes, which might even influence the results at rather late times.[14] Furthermore, in Eq. (37) we neglected any radial dependence of D_A and β which might give a similar effect. In this case Eq. (21) reads:

$$\partial n_-/\partial t = \nabla^2 D_A(t) \cdot n_- - \beta(r,t) n_-. \tag{38}$$

THE PLANE-WAVE ASSUMPTION

The basic assumption on which essentially every free-space interferometer technique is based is that the horns transmit and receive a well-collimated plane wave. Then, the measurements define simply an integrated index of refraction that can be interpreted as discussed previously.

This plane-wave condition is only an approximation the quality of which depends on the radiation pattern of the transmitter and receiver, on the location of the plasma between the horns (near field-far field), and on the dens action of glass container and plasma (ratio of plasma diameter to beam width). To estimate the errors involved in this approximation and to give an improved analysis, we would first have to describe the field pattern of the transmitting antenna in the near field region and in the transition region between near field and far field, because the plasma is usually placed

[12] M. A. Biondi and S. C. Brown, Phys. Rev. 75, 1700 (1949).
[13] A. W. Engel and M. Steenbeck, *Elektrische Gasentladungen* (Springer-Verlag, Berlin, 1944), Vol. II.
[14] Another explanation of the curvature stems from the fact that the amplitude of the measuring wave is not constant but changes with time, and Eq. (7) should be correctly used instead of Eq. (3). The deviation caused by this effect should be considerably smaller, however, and would be almost zero for late times, since the amplitude changes very little then, but the representative Fig. 8 shows that the last point ($l=k$) is regularly somewhat above the straight line, indicating that the curvature exists even there.

FIG. 10. (a) Pattern of the transmission channel with glass; (b) pattern of the transmission channel without glass.

in this region. Secondly, this radiation pattern has to be analyzed in terms of the receiving antenna, because it sees only what "fits" in its radiation pattern. A possible interaction between transmitting and receiving horn has also to be taken into account. A mathematical treatment of this problem, even without lens action included, has not yet been given, as far as the authors know, and without doubt the mathematical implications are formidable. To explore the situation we have therefore tried to attack this problem by an experimental method.[15] We simulate the plasma by a small rotating dielectric probe and scan the field pattern between the horns, in this way studying the influence of a particular volume element (defined by the geometry and the location of the probe) on the received signal. In Figs. 10(a) and 10(b) we show a number of cross sections of the transmission channel, which have been used in the actual measurements and get the following results: The pattern of the transmission channel does not change much between transmitter and receiver, only small side lobes are present; the width of the transmission pattern is approximately constant and about equal to the width of the horns; the glass of the discharge tube does not influence the pattern very much if the system has been carefully aligned. These results seem to indicate that the beam is indeed well collimated, and the errors arising from the plane wave assumption cannot be great.

In the actual measurement the rotating probe is replaced by the plasma. Only if $\lambda_0 \ll$ beam width D of the incident wave $\ll$ plasma diameter $2R$, will the plasma be an effective slab and can the lens action of the plasma be neglected. Because of experimental limitations the ratio $2R/D$ cannot be made arbitrarily large (approximately 5 in our case), and the plasma acts more or less as a time-varying lens almost in any situation. Measurements in which we moved the receiving horn around the plasma do not indicate a pronounced effect. The lens effect has been calculated in the optical approximation too, and the application of the results to our case again indicates only small errors, especially for late times.[16]

We feel that both these results show that the given interpretation of the measurements is based on reasonable assumptions. However, much must be done to express our argument quantitatively.

We would like to mention two experimental alternatives: An interferometer setup similar to a Fabry-Perot arrangement[17] will lead to a highly plane wave. The introduction of cylindrical lenses and placement of the plasma in their focal line[18] will possibly avoid any lens action of the plasma. The first method seems to be limited by the losses within the plasma, the second by the quality of the lenses. A combination of both might remove the entire problem.

CONCLUSION

The measurement of the integrated index of refraction and its change with time can be successfully used to study very accurately the loss processes in a decaying plasma. In our experiment, the electron losses are mainly due to ambipolar diffusion and attachment. Additional measurements in the presence of a magnetic field seem to allow a separation of both loss processes. Mass spectrometric measurements are planned which should lead to a unique interpretation of the results.

ACKNOWLEDGMENTS

The authors gratefully acknowledge the assistance of P. Wolfert, Dr. W. J. Ramm, J. J. Sullivan, and I. A. Balton.

[15] P. Wolfert, "Measurement and Discussion of the Differential Microwave Beam between Two Horn Antennas as Used in Microwave Plasma Diagnostics," USASRDL Technical Report (in preparation).

[16] J. Shmoys, Research Report PIBMRI-828-60, Microwave Research Institute, Polytechnic Institute of Brooklyn (1960).

[17] W. Culshaw, Proc. Phys. Soc. (London) B66, 597 (1953).

[18] A. L. Gardner, University of California Lab. Report UCRL-6232-T.